

## The International Journal of Engineering and Information Technology (IJEIT)



# Classification of Malignant and Benign Skin Lesions Using CNN Models

Ahmed J. Abougarair<sup>1,\*</sup>, a.abougarair@uot.edu.ly, Osama Abolaeha<sup>2</sup>, abolaeha@gmail.com

Mohamed K. Aburakhis<sup>3</sup>, aburakhism1@gmail.com

1,2,3 Electrical and Electronics Engineering Department, University of Tripoli, Tripoli, Libya

\* Corresponding author

#### Article History

Received 04 Jul, 2025 Revised 23 Sep, 2025 Accepted 09 Nov, 2025 Online 25 Nov, 2025 DOI:

https://doi.org/10.36602/ijeit.v14i1.572

#### **Index Terms**

accuracy, cancer detection, deep learning, performance, skin lesions.

#### Abstract

Dermatology has been transformed through the use of machine learning in health research. By leveraging large data sets and training deep learning models on diverse skin lesion images, researchers have opened the door to improving and modernizing traditional diagnostic methods. This paper aimed to develop a highly effective model for accurately classifying skin cancer images as benign or malignant, thus contributing to early detection. The methodology involved utilizing three custom Convolutional Neural Networks (CNNs) to extract essential features from dermatoscopic images, focusing on characteristics such as the borders of melanoma. Non-cancerous tumors are typically smooth and regular in their edges, while malignant ones have an uneven and rough border. The CNN models were trained on a melanoma dataset comprising images from both benign and malignant cases. Pre-processing steps such as data augmentation were also employed to further improve the performance of the model. The performance of the models was evaluated thoroughly using metrics such as precision, recall, F1 score, and accuracy. By training the models on Melanoma skin cancer, the models provided relatively high accuracies on the validations: 91%, 88%, and 94% for the first, second, and third model, respectively. Additionally, the accuracy for Benign skin cancer is 92%, 89% and 95% for the first, second, and third model, respectively. The third CNN model achieved the best precision and recall with 93% and 95% for Benign skin cancer, and 92% and 94% for Melanoma skin cancer. The third CNN model consistently outperformed the others, offering balanced and superior accuracy in distinguishing between benign and malignant skin cancer cases.

### تصنيف الأورام الجلدية الخبيثة والحميدة باستخدام نماذج الشبكات العصبية الالتفافية

أحمد ابوجرير  $^{1*}$ ، أسامة ابولايحة  $^{2}$ ، محمد ابورخيص أحمد الكهربائية والالكترونية، جامعة طرابلس، طرابلس، ليبيا  $^{3\cdot2\cdot1}$  قسم الهندسة الكهربائية والالكترونية، جامعة طرابلس

الكلمات المفتاحية

الملخص

الدقة، اكتشاف السرطان، التعلم العميق، الأداء، آفات الجلد يشهد طب الجلدية تطوراً ملحوظاً بفضل التعلم الألي، حيث ساعدت النماذج العميقة والبيانات الكبيرة في تعزيز الطرق التقليدية للتشخيصر تهدف هذه الورقة تطوير نموذج فعال لتصنيف صور سرطان الجلد بدقة إلى فنتين: سرطان حميد وخبيث، مما يساهم في تعزيز جهود الكشف المبكر. اعتمدت المنهجية على استخدام ثلاثة نماذج مخصصة من الشبكات العصبية الالتفافية (CNN) لاستخراج الخصائص المهمة من صور الجلد الملخوذة بالدرماتوسكوب، مع التركيز بشكل خاص على خصائص حدود الورم الميلانيني. فعادةً ما تتميّز الأورام الحميدة بحواف ناعمة ومنتظمة، بينما تظهر الأورام الخبيثة حدودًا غير منتظمة وخشنة. تم تدريب نماذج الشبكات العصبية الدلامات على مجموعة بيانات تضم صورًا لحالات العبيثة، كما تم تطبيق عمليات معالجة مسبقة، مثل زيادة البيانات، لتحسين أداء النماذج. وقد جرى تقييم أداء النماذج باستخدام مقاييس معيارية تشمل الدقة الإيجابية (precision)، الاسترجاع (eccall)، درجة 11، ونسبة الدقة. حقق النماذج بالشائد الميلانوما على التوالي. أما بالنسبة لتصنيف الحالات الحميدة، فبلغت 11%، 88%، و94% في تصنيف حالات الميلانوما على الأداء المؤضل، حيث حقق قيم دقة واسترجاع بلغت 93% و 95%، و95%، و95% و95% لحالات الميلانوما، وبشكل عام الخميدة النامذج باستمرار على النموذجين الأخرين، وقدم أداء متوازنًا وممتازًا في التمييز بين الأورام الحميدة.

#### I. INTRODUCTION

In recent years, the incidence of skin cancer has risen significantly, raising global concern. Skin cancer originates from abnormal cell growth in the skin, and when this growth becomes uncontrolled, it leads to cancer. Skin cancer is one of the most common types of cancer worldwide, mainly due to prolonged radiation from ultraviolet sunrays [1]. Since skin is the largest organ in the human body, the trends in skin cancer are not surprising. Skin cancers are usually classified into three major types, including melanoma, SCC (squamous cell carcinoma), and BCC (basal cell carcinoma). Among these three, melanoma has the highest death rate. It originates from melanocytes, the melanin-producing skin cells responsible for skin color. The mortality rate for melanoma is about 2% when it is in its early stage but increases exponentially to 38% if disseminated to lymph nodes and further to 84% with disease progression beyond this point [2,3]. Given that skin cancer typically spreads slowly, early-stage detection makes it more treatable, and melanoma is highly curable if caught early [4]. However, diagnosing skin cancer remains challenging and costly, with annual medical expenses associated with skin cancer increasing by 26.2%, compared to just 25.1% for other types of cancer [5]. This economic burden makes the early detection of skin cancer a key area of interest worldwide.

Recent developments in technology, especially in AI and computer vision, have introduced new ways of diagnosing cancer. AI is defined as the process of using computers to perform intelligent tasks using a minimum of human input [6]. Among various ML techniques, DNNs have been very successful in processing large training datasets, which require huge computational resources, usually performed by GPUs. Convolutional Neural Networks have gained wide attention in medical imaging because of their great capability in handling large datasets and their efficient usage of resources. Recent years have witnessed significant competition between deep learning techniques, like CNNs, and low-level object representation methods for applications in image detection [7]. CNNs have emerged as a powerful aid in medical image analysis, facilitating precise malignant and benign skin lesion discrimination through automatic feature extraction and classification. Deep learning technologies are employed by the models in the analysis of extensive skin image databases, enhancing the accuracy of diagnoses and potentially reducing the workload of dermatologists. The application of CNNs in dermatology not only enhances the pace of diagnosis but also early detection, which plays a critical role in successful treatment outcomes. CNNs' ability to learn from large amounts of data allows them to identify small patterns and characteristics, which might be overlooked by the human eye, leading to more precise analyses of skin disorders. This healthcare technology advance is a giant leap towards personalized medicine as it enables health care professionals to provide evidencebased practice decisions informed by data-driven facts [8]. A sequential CNN architecture was employed for

pre-processing images, discriminating areas of interest, and detection of features. It achieved 96.25% accuracy on HAM 10,000 database, which was higher compared to other models like VGG 19 and ResNet-50 [9]. SkinNet1 and SkinNet2 were introduced, where SkinNet2 combined deep learning with Support Vector Machine (SVM) for improving accuracy. SkinNet2 achieved 92% accuracy through a test set [10]. The DenseNet201 model was enhanced and had a sensitivity of 93.96% and specificity of 97.03%, which illustrates its accuracy in distinguishing malignant and benign lesions [11]. A ResNet50-SVM framework got area under the ROC curve of 99.52% and accuracy of 99.87% [12]. CNN models have produced outstanding accuracy in skin lesion classification. A CNN model trained using 10,000 images achieved 95% accuracy on the test set [13]. A customized CNN architecture achieved 85% F1-score and 83% ROC- AUC and performed extremely well when implemented on the ISIC dataset [14]. The VGG16 and ResNet50 models that use transfer learning were compared, and VGG16 achieved 87% accuracy and surpassed other models [15]. Generalization of the model was improved through techniques such as image resizing, normalization, and data augmentation. For example, data augmentation included random flipping and zooming to increase dataset diversity [16]. Both pre-trained MobileNetV2 and ResNet50 were fine- tuned to classify skin lesions, where the accuracy achieved using MobileNetV2 was 92.97% [17]. The heterogeneity of skin lesion datasets, particularly for skin colors and lesion types, remains an issue. Models may vary on datasets with underrepresented darker skin colors [18]. The CNNs have shown promising performance in classifying malignant and benign lesions with high accuracy and stable performance on varied datasets. Deep learning with medical imaging can revolutionize dermatological diagnosis, enabling early detection and better patient outcomes. Table 1 and 2 illustrate the performance comparison of CNN models for different studies. Future research should focus on dataset diversity and model architecture optimization for even better performance.

TABLE I. PERFORMANCE COMPARISON OF CNN MODELS

| <b>Model Architecture</b> | Accuracy (%) | Ref  |
|---------------------------|--------------|------|
| Sequential CNN            | 96.25        | [9]  |
| SkinNet2                  | 92           | [10] |
| Modified<br>DenseNet201   | 95.50        | [11] |
| ResNet50 with SVM         | 99.87        | [12] |
| VGG16                     | 87           | [14] |
| MobileNetV2               | 92.97        | [17] |

TABLE II. SUMMARY OF MALIGNANT AND BENIGN SKIN RESEARCH STUDIES

| Ref   | Summary  |
|-------|--|
|       | The proposed deep sequential CNN model was 96.25%  |
|       | accurate in classifying the skin lesion as malignant or  |
| [9]   | benign, outperforming other models like CNN transfer   |
|       | learning (87.9%) and VGG 19 (86%), indicating  |
|       | significant improvements in skin lesion classification. The study presents two models, SkinNet1 and SkinNet2,      |
|       | using CNN to classify dermoscopy images as melanoma  |
| [10]  | and benign. SkinNet1 uses deep learning  |
| []    | exclusively, and SkinNet2 uses acombination of deep  |
|       | learning and SVM to classify the images with 90.5% and   |
|       | 92% accuracies, respectively.  |
|       | The study uses tailored MobileNetV2 and DenseNet201  |
| [11]  | models to classify skin lesions into malignant and benign<br>classes with 95.50% accuracy, 93.96% sensitivity, and |
|       | 97.03% specificity for detecting skin cancer.  |
|       | The study compares various pretrained CNNs like VGG-   |
|       | 16, ResNet50, and InceptionV3 for classification of  |
| [12]  | malignant melanoma and benign skin lesions with  |
|       | improved performance utilizing ResNet50 with Support   |
|       | Vector Machine to gain 99.87% accuracy.  |
|       | The study developed a better DNNs for the diagnosis of<br>skin lesions as benign or malignant with an 84% success  |
| [14]  | rate using the Adam optimizer, from a dataset of 3,297   |
|       | dermoscopic images for accurate diagnosis.   |
|       | The study constructed convolutional neural network   |
| F4 =3 | models VGG16 and VGG19 for the classification of skin  |
| [15]  | lesions into malignant and benign classes. VGG16   |
|       | achieved the best accuracy of 87%, outperforming the custom CNN model in this binary classification.               |
|       | The work employs a modified convolutional neural   |
|       | network (MOCNN) to accurately classify skin lesions as   |
| [16]  | malignant or benign at 91.62% in a model trained on  |
| [10]  | 10,540 images with the added benefit of data   |
|       | augmentation for the robustness and generalizability of  |
|       | the model.  The study utilizes a CNN model based on MobileNetV2  |
|       | for classifying malignant and benign skin lesions,   |
| F177  | achieving high accuracy of 92.97%, with metrics like   |
| [17]  | recall (92.71%), precision (94.70%), and F1 score  |
|       | (93.47%) indicating its effectiveness in skin cancer   |
|       | diagnosis.  The study utilizes a CNN model in MobileNetV2 for the  |
|       | classification of malignant and benign skin lesions with an  |
| F107  | accuracy of 92.97% and other indicators like recall  |
| [18]  | (92.71%), precision (94.70%), and F1 score (93.47%)  |
|       | indicating its effectiveness for the diagnosis of skin   |
|       | cancer.  |
|       | The article presents a CNN model to identify skin cancer lesions as malignant or benign with around 92% accuracy   |
| [19]  | for the training set and over 95% accuracy for the test set,   |
|       | demonstrating successful early detection.  |
|       | The study utilized CNN to distinguish between malignant  |
|       | and benign skin lesions based on the ISIC2018 dataset.   |
| [20]  | The CNN model outperformed other transfer learning   |
|       | models with a 85.8% accuracy, which demonstrated effective discrimination between lesion types.                    |
|       | The study developed computer models by using pre-  |
|       | trained convolution neural networks to categorize skin   |
| [21]  | lesions into benign and malignant. An accuracy of 94%  |
|       | and 93% was achieved with the model DenseNet121,   |
|       | while EfficientNet B0 categorized nine classes of skin   |
|       | tumors accurately.   |
|       | The work employs CNN to differentiate 1497 cancerous and 1800 non-cancerous skin lesions with 92.7%                |
| [22]  | and 1800 non-cancerous skin lesions with 92.7% precision. Balanced dataset and the ResNet50 architecture           |
|       | enhance the model's accuracy in detecting skin cancer.   |
|       | The research evaluates a proposed CNN model for lung   |
| [23]  | cancer image classification with 99.9% to 100% accuracy  |
|       | in distinguishing between benign and malignant lesions   |
|       | based on the LC25000 dataset of 10,000 labeled images to   |

enable automatic effective detection of cancer.

| [24] | The article explores the application of CNNs in the classification of malignant melanomasand benign lesions, and how they can be used to improve accuracy and reliability in melanoma detection, leading to better patient outcomes and treatment effectiveness in clinical practice.                              |
|------|--|
| [25] | The article proposes a deep CNN for the classification of breast lesions into malignant and benign with a training accuracy of 0.98 and test accuracy of 0.97, significantly reducing human error in mammography interpretation and diagnosis.   |
| [26] | The study uses a residual network (ResNet-50) as a deep learning CNN for skin lesion classification and achieves over 97% accuracy in the classification of benign to malignant categories using 320 clinical images for training.   |
| [27] | The study compares the Novel Densely Connected Convolutional Network CNN in the classification of malignant and benign skin lesions with detection rates of 80.8% and 76.3% respectively, statistical significance attesting to the superiority of the former's detection efficacy.                                |
| [28] | The study uses a one-dimensional convolutional neural network to separate malignant and benign tumors with 99.9% classification and 98.8% ROC- AUC. Experimental data of new tumors should be carried out to validate the model's performance.   |
| [29] | The article presents a skin lesion classification model based on Efficient Net B7 CNN architecture that achieves 87% accuracy in distinguishing malignant from benign lesions across eight classes, including Basal Cell Carcinoma, Squamous Cell Carcinoma, and Melanoma, from images captured by mobile cameras. |

In this paper, three CNN models were employed to extract critical features from dermatoscopic images of skin lesions, such as the borders of melanoma. Benign tumors typically have smooth borders, while malignant tumors exhibit irregular, rough edges. These models were trained on a common dataset, enabling direct comparison of their performance in classifying benign and malignant lesions. The present paper is dedicated to the development of CNN models for skin cancer detection, training those models on the Melanoma Skin Cancer Dataset, and evaluating and comparing their training accuracy with respect to the chosen dataset.

#### II. DATASET AND METHODOLOGY

In this section, Melanoma skin cancer detection system has been implemented to distinction between Benign and Malignant skin tumors. The implemented system utilized three different CNN models with the same dataset as an input. The flow chart in Fig. 1 summarizes the important steps and provides a visual representation of the essential elements and the overall procedure [30, 31].



Figure 1. A flow chart demonstrating the essential steps

#### A. Data Preparation

The necessary data for this paper were collected from Kaggle website [32]. Melanoma skin cancer dataset contains exactly 10602 dermatoscopic images of pigmented skin lesions which are distributed as 5499 images for Benign tumor and 5103 images for Malignant

tumor. The images included in the dataset have dimensions of  $300 \times 300$  and 3 channels due to its color mode "RGB". Figures 2 and 3 shows samples of the dataset.

#### B. Data Splitting

As mentioned before, the dataset consists of 10602 images. The data is categorized in such a way that 10% of the data is carried in the test data while the other 90% is carried in the train data. However, the train data itself has been splitted to obtain 25% to validation as shown in Table 3 and Fig. 4.

TABLE III. THE DISTRIBUTION OF DATA TO BE TRAINED

| Class      | Benign | Malignant | Total |
|------------|--------|-----------|-------|
| Test       | 499    | 499       | 998   |
| Train      | 3750   | 3453      | 7203  |
| Validation | 1250   | 1151      | 2401  |
| Total      | 5499   | 5103      | 10602 |

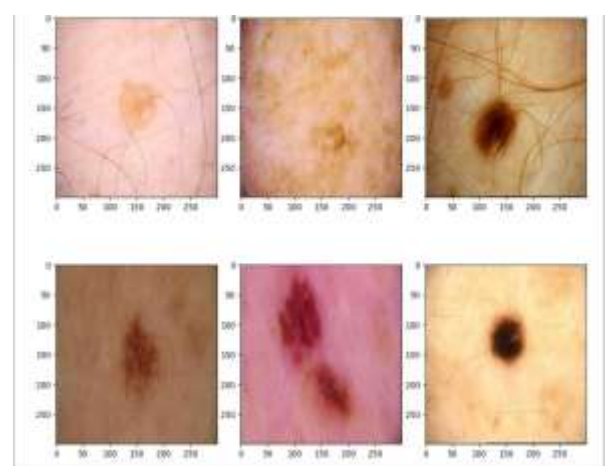


Figure 2. Benign samples of the dataset [32]

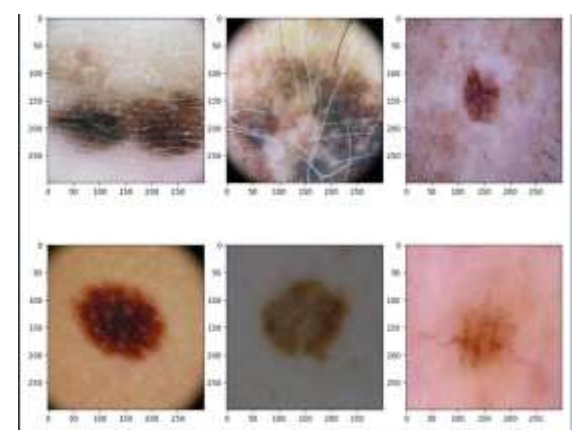


Figure 3. Malignant samples of the dataset [32]

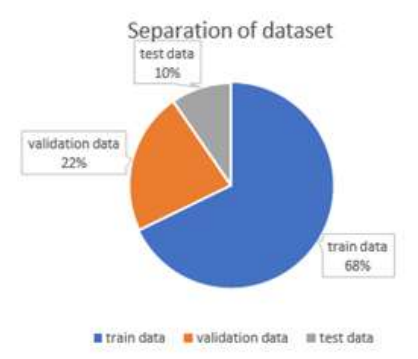


Figure 4. The distribution of data to be trained

#### C. Training Phase

In this paper, three different CNN models were used for training with different structures such as number of convolution layers, arranging of layers and number of neurons in the FC layers. All three models are custom CNN architecture, and no pre-trained models were used. Figure 5 represents the block diagram of training phase [33-35].



Figure 5. Block diagram of training phase

Image reading: The implemented system uploaded the data from a directory dataset. Which was then utilized for training in the next stages which is executed on Jupiter notebook via Kaggle website using GPU P100 accelerator to run the Keras library. The system enhances images and generates new images for training datasets in order to produce additional samples before feeding them to the CNN models. The pre-processing techniques used in the implemented system are indicated in Figure 6.

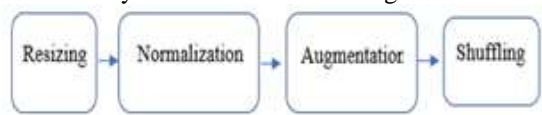


Figure 6. A flow chart of data pre-processing

Image resizing: Prior to the training phase, the images are adjusted to a fixed size of 224x224 pixels in 'RGB' color format. This resizing reduces dimensionality and computational demands, enabling the network to perform more efficiently with simpler calculations while maintaining accuracy. Figure 7 illustrates an example of an input image both before and after the resizing process. Normalization: The pixel values of the images are normalized to the range [0, 1] by dividing each pixel intensity by 255. This standardization is a common preprocessing technique in neural network training to ensure consistent input scaling.

Data Augmentation: To train a model with many trainable parameters and achieve competitive performance a significant volume of images is required. Image augmentation has been demonstrated to be an effective and efficient solution to this problem. Data augmentation is a technique for increasing the number of images for underrepresented groups without suffering the

cost of additional image collection. For object recognition and image categorization, several image augmentation techniques have been used such as: crop, flip, intensity changing, translate, elastic distortion, cutout, mix-up and rotation [36]. For the implemented system, the images were randomly rotated by up to 20 degrees as shown in Figure 8. In addition, the images were horizontally flipped as shown in Figure 9. The augmentation process adds diversity to the training data and improves the model's ability to generalize to different object orientations.

*Shuffling:* The input data were grouped into batches with a specified batch size (64) where each batch is trained individually. The images were shuffled before each epoch to prevent overfitting and provide randomity.

#### III. TRAINING PROCESS

In this process, all three custom CNN models were built and compiled to be trained on the Melanoma skin cancer dataset. All models are discussed below [37-40]. After building and compiling each model, the models were saved for future use. Models that have been saved can be used to make predictions on new data without needing to be retrained since the learnt weights, biases, and architecture are preserved.

#### A. The first model

The first utilized model was a custom CNN sequential model consisting of two convolution layers each followed with a max pooling layer and a drop out layer. Fig. 10 reveals each layer in the first model. The first 2D convolution layer has 64, kernel size of 3x3, filter to obtain the convolution operation with the (224x224x3) input, the activation function used in this layer was Leaky ReLU to obtain nonlinear operations. 10% of the neurons in this layer drop out to prevent overfitting.

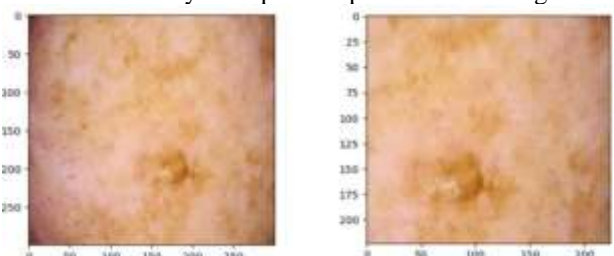


Figure 7. The effect of image resizing

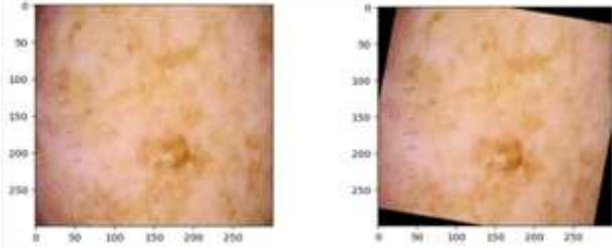


Figure 8. The effect of image rotation

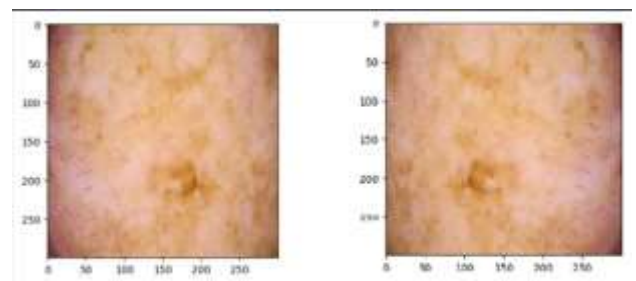


Figure 9. The effect of image flipping

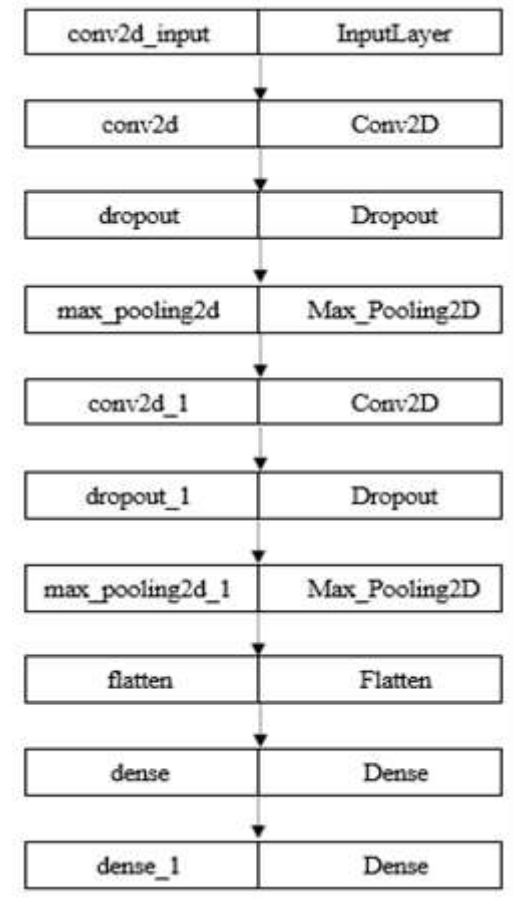


Figure 10. Layers in the first model

A max pooling layer is obtained to detect the most important features. A second 2D convolution is applied while this layer has 128 filters with the same kernel size of 3x3. The dropout obtained for this layer was 15% and followed with another max pooling layer. A flatten layer is obtained to convert the 2D input to a 1D vector, this expands the data for the afterwards FC layer. The first FC layer is considered as an input layer of the FC layer stage which has 256 neurons. The second FC layer is considered as the final FC layer that consists of 2 neurons responsible for the classification, and the used activation function in this layer was Sigmoid which is suitable for the binary classification.

#### B. The second model

The second utilized model was also a custom CNN sequential model consisting of four similar blocks, where each block consists of convolution layers with drop out and max pooling layers varying in the number of filters

and neurons. Figure 11 reveals each layer in the second model. This model has four different blocks, where each block consists of a 2D convolution layer associated with drop out and a max pooling layer. The first block has 64 filters for the convolution layer each of 3x3 kernel size, and 10% of the units were dropped out. The second block has 128 filters with a size of 3x3, 15% of the neurons were set to 0. For the third block, the convolution layer has 256 of 3x3 kernels and 20% of the neurons were randomly selected to be dropped out, reducing the model's reliance on specific features. The convolution layer of the fourth block consists of 512 filters each of 3x3 kernel size and 30% of the neurons were dropped out to prevent overfitting. All previous convolution layers used Leaky ReLU activation function and followed by a max pooling layer. A flatten layer follows the last max pooling layer to convert the 2D input to a 1D vector 1024 neuros layer is considered as an input to the FC layer. Followed by 2 neurons classifier layer with Sigmoid activation function which is considered as an output of the FC layer.

#### C. The third model

The third utilized model was a custom CNN sequential model which also consists of four convolution layers. However, these layers are allocated so that every pair of subsequent layers and a max pooling layer performs a block. Figure 12 reveals each layer in the third model. The third model is a sequential model that starts with a 2D convolution layer of 64 filters of 3x3 kernel size and a padding parameter that sets the output to have the same spatial dimensions of the input, this layer is followed by another 2D convolution layer having the same parameters. Both of the convolution layers use Leaky ReLU activation function. This pair of convolution layers is followed by a 3x3 sized max pooling layer which is provided to reduce the spatial dimensions of the input. A second block consists of the same layers as the previous block with the same parameters except that the convolution layers in the second block have 128 filters for each layer. The output is converted from 2D to 1D vector in the subsequent stage by applying a flatten layer. Next, a 256-unit input layer that uses the Leaky ReLU activation function is given to the dense layer (FC layer). After that, a drop out layer is introduced with a 50% drop out rate. The second dense layer, which is the last FC layer has two neurons involved in categorization, was activated using the sigmoid function.

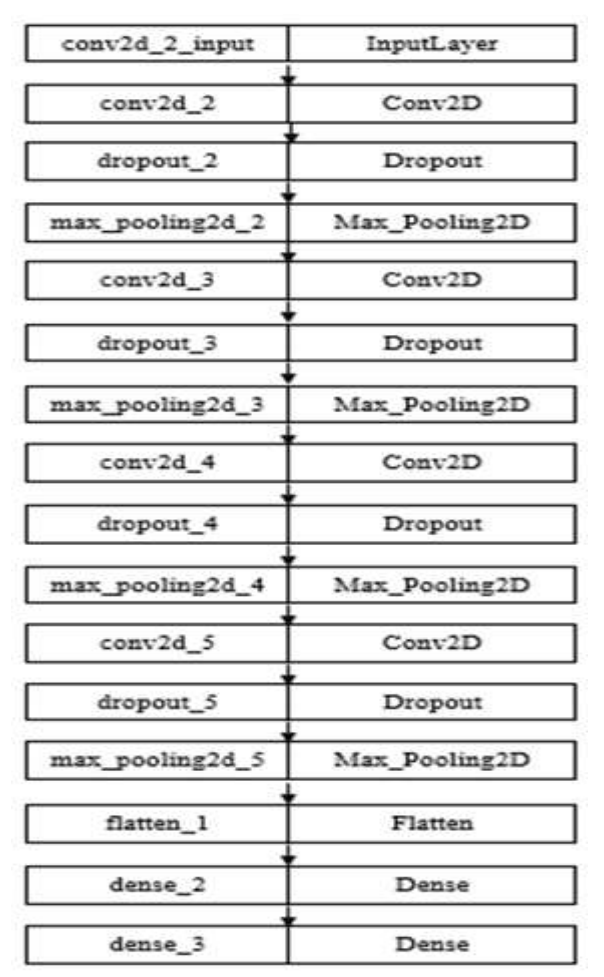


Figure 11. Layers in second model

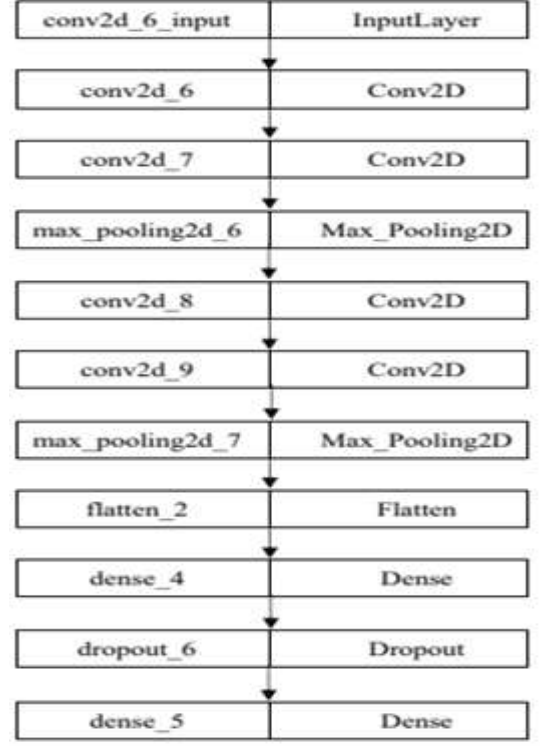


Figure 12. Layers in the third model

Testing had to be performed through a set of images that are distinct from those which were used to train the model in order to assess the model's performance. Testing has been done by loading a random image from the dataset to serve as an input for the model, to preprocess the image, it has been resized to the dimensions of (224,224) to ensure that the image is compatible with the input size expected by the model, converting it to a NumPy array which is a common data structure used for numerical computations in DL, finally a normalization has been done by dividing the pixels on 255. The required model has been loaded in order to predict the image's class.

The predicted skin cancer class is displayed in a simple manner for the user to understand without having to examine the specific predictions extensively, by creating visual representations of the input image associated with the predicted class and an indication of which prediction is correct or incorrect. A sample of the test images were entered into the system and Figures 13, 14, 15, and 16 shows samples of the results of correctly recognized Malignant cancer, correctly recognized Benign cancer, incorrectly recognized Malignant cancer and incorrectly recognized Benign cancer respectively in the testing phase.





Figure 13. A sample of correctly recognized malignant cancer



Figure 14. A sample of correctly recognized benign cancer



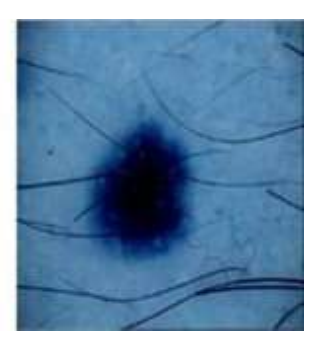


Figure 15. Samples of the incorrectly recognized malignant cancer

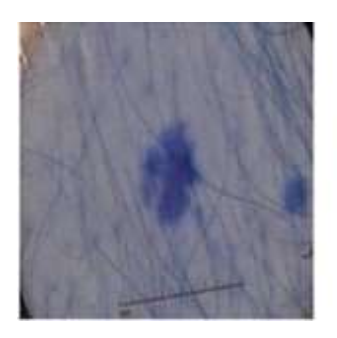




Figure 16. Samples of the incorrectly recognized benign cancer

#### IV. SIMULATION RESULTS

For Melanoma skin cancer detection, three CNN models were used to compare the structures and the consisting neurons in the models with their corresponding accuracies to classify a dermatoscopic skin lesion of which is a Benign or Malignant skin cancer. The performance analysis of the chosen models was provided and properly covered. The performance evaluation process has been applied in the same way for all systems. Table 4 describes the configurations used to evaluate and compare the performance of the utilized models.

TABLE IV. EVALUATIONS CONFIGURATIONS OF THE MODELS

| Loss Function | Categorical Loss Entropy                 |
|---------------|--|
| Optimizer     | Adam                                     |
| Performance   | Accuracy, Precision, Recall and F1 score |

All three models were modified and then employed to train on Melanoma skin cancer dataset. The modified models were trained for only 10 epochs with monitoring the accuracy and loss of each epoch for the three models in order to observe the corresponding enhancement in accuracy of every modification in the system [41-43]. The original system was operating with 64 batch size, soft max activation function in the classifier layers, ReLU activation function in the convolution layers. 5 indicates each modification with the corresponding train accuracy, validation accuracy, train loss and validation loss of each model after 10 epochs. It appeared that all the modification in the system hyperparameters has led to an improvement in performance for all models, except for reducing the batch size to 32 where it resulted in reducing the validation accuracy of the first and second models along

with a significant increase in the losses of these models. However, reducing the batch size to 32 positively affected the third model. Thus, it was not sufficient to make such a trade-off. As a result, all the modifications mentioned in the previous table were adopted except for decreasing the batch size. This paper prepared using MATLAB [44-48] for data analysis, simulations, and visualization. All computational results, figures, and algorithms presented herein were generated using MATLAB [49-57].

TABLE V. THE IMPROVEMENTS OF THE SYSTEM

| Type of modification   | Model | Train<br>Accuracy | Train<br>loss | Val<br>Accuracy | Val<br>loss |
|------------------------|-------|-------------------|---------------|-----------------|-------------|
|                        | 1     | 83                | 0.5           | 86              | 0.4         |
| Original system        | 2     | 62                | 0.61          | 59              | 0.25        |
|                        | 3     | 87                | 0.29          | 89              | 0.69        |
| Convert the activation | 1     | 87                | 0.29          | 84              | 0.48        |
| functions from         | 2     | 63                | 0.6           | 61              | 2.14        |
| soft-max to<br>sigmoid | 3     | 87                | 0.29          | 89              | 0.25        |
| Convert the activation | 1     | 89                | 0.25          | 88              | 0.26        |
| functions From         | 2     | 88                | 0.27          | 87              | 0.4         |
| ReLU to<br>Leaky- ReLU | 3     | 89                | 0.26          | 90              | 0.23        |
| Reducing               | 1     | 89                | 0.25          | 81              | 0.47        |
| Batch size             | 2     | 88                | 0.25          | 86              | 0.44        |
| from 64 to 32          | 3     | 90                | 0.23          | 90              | 0.21        |
| Doubling               | 1     | 88                | 0.27          | 90              | 0.25        |
| number of              | 2     | 88                | 0.26          | 82              | 0.5         |
| neurons in each layer  | 3     | 91                | 0.22          | 89              | 0.26        |

#### A. Results of the training phase

The modified DL models were trained for 35 epochs with monitoring the results of each epoch. This training process was done using the Melanoma skin cancer dataset. All three models showed an improvement in the accuracy of the training data which illustrates the effectiveness of the DL models that have been utilized.

#### 1. Results of training of the first mode

The first model was trained for 35 epochs, and the final train accuracy has reached 91.38%. However, the validation accuracy of the final epoch has reached 90.92%. Figures 17 and 18 indicates a plot of the learning process for each epoch in terms of accuracy and loss respectively. The two figures reveal increasing in both train and validation accuracy curves. Conversely, the train loss and validation loss curves are decreased through the learning process. The two figures share the fact that the train and validation curves are dispersed until the 11th epoch where the curves intersect. After that the curves oscillate decreasingly attempting to reach the steady state. Performance dipped slightly between epochs 22–25 before recovering. However, this obstacle has been resolved in the following epochs. The first epoch's train accuracy, validation accuracy, train loss, and validation loss were respectively 70.42%, 48.02%, 3.63, and 5.67. These values were enhanced, giving the final epoch values to 91.38%, 90.92%, 0.21, and 0.24 respectively. Figure 19 illustrates the confusion matrix of the first model. The first model accurately identified 713 instances of Malignant Melanoma. It correctly classified 438 instances as Benign. However, it misclassified 1219 instances as Malignant when they were actually Benign. Additionally, the model failed to identify 31 instances of Malignant tumors.

#### 2. Results of training the second model

The second model was trained for 35 epochs, and the final train accuracy has reached 92.18%. where the validation accuracy of the final epoch has reached 88.30%. Figure 20 indicates a plot of the train and validation accuracy as a function of the training epochs of the second model. Figure 21 indicates a plot of the train and validation loss as a function of the training epochs of the second model. The plot indicates that both accuracy curves are rising which indicates improvement in the learning process. It is observed that the accuracy improvement of the second model through the learning process is more stable than the first model. where the curves' disparity is significantly less, either before or after the 11th epoch. Train accuracy and validation accuracy for the first epoch were 69.75% and 66.81%, respectively. After 35 epochs, these percentages resulted in final epoch values of 92.18% and 88.3%, respectively. Figure 21 shows the significant disparity between the train and validation loss curves due to the oscillation of the validation curve. However, both loss curves are falling, demonstrating progress in the learning process. Train loss and validation loss of the initial epoch were 0.82 and 0.77, respectively. Through the learning process, these values kept falling to reach 0.19 and 0.52, respectively in the final epoch. Figure 22 illustrates the confusion matrix of the second model. The second model correctly detected 953 cases of Malignant cancers and 198 cases as Benign. In the other hand, 1198 cases were incorrectly identified as cancer while they were Benign, and 52 cases of Malignant tumors were missed by the model by identifying them as Benign.

#### 3. Results of training the third model

The third model was trained for 35 epochs, reaching a final training accuracy of 92.18% and a validation accuracy of 88.30% in the last epoch, outperforming all other models discussed in this paper. Figure 23 display train and validation accuracy plotted against the training epochs of the third model. Figure 24 present train and validation loss over the training epochs of the third model. similar to the past 2 models, train accuracy and validation accuracy curves are growing while the train and validation loss curves are dropping through the training process. It is noted that the primary epoch's train accuracy, validation accuracy, train loss, and validation loss were respectively, 76.76%, 85.92%, 0.48, and 0.35. These values were improved, resulting in 35th epoch values of 93.28%, 82.88%, 0.17, and 0.18, respectively.

These results reflect that the learning progress of this model is the slowest among the utilized models. Despite this, it produces the best final outcomes. The most notable aspect of the third model train and validation

curves is the stable slow improvement in both accuracy and loss performance, exhibiting a remarkable level of semi-identicality, which implies that the model is effectively capturing patterns and relationships in the training data without overfitting or excessively memorizing specific examples. Figure 25 illustrates the confusion matrix of the third model. The third model accurately identified 1022 instances of Malignant Melanoma. It correctly classified 129 instances as Benign. However, it misclassified 1180 instances as Malignant when they were actually Benign. Finally, the model failed to identify 70 instances of Malignant tumors.

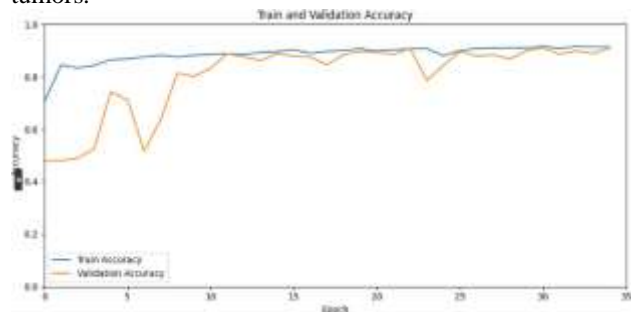


Figure 17. Accuracy curves as a function of training epochs for the first model

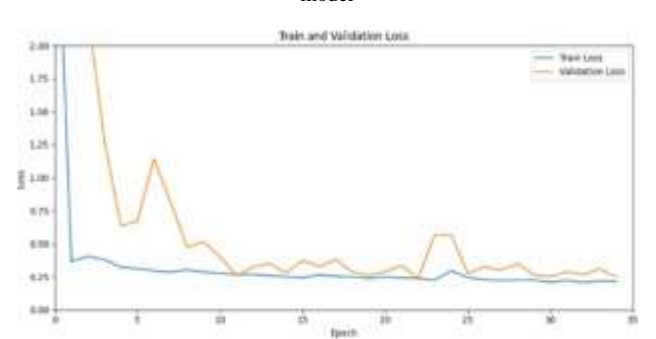


Figure 18. Loss curves as a function of training epochs for the first model

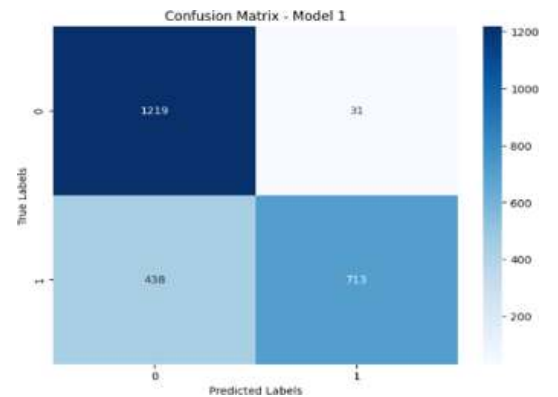


Figure 19. Confusion matrix of the first model

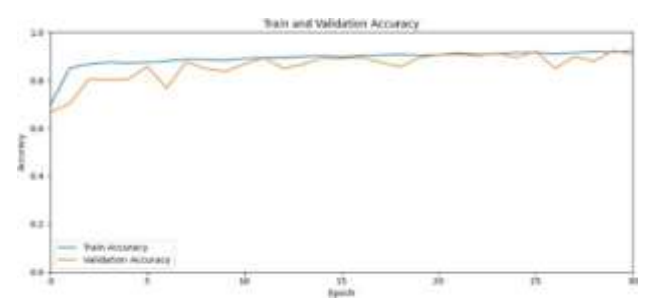


Figure 20. Accuracy curves as a function of training epochs for the second model

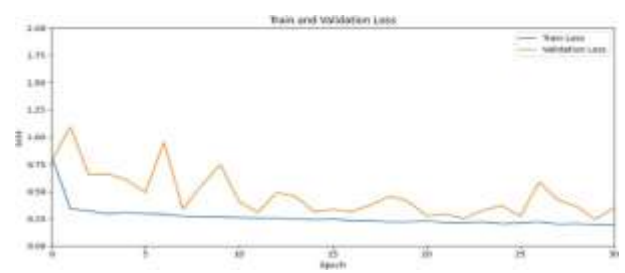


Figure 21. Loss curves as a function of training epochs for the second model

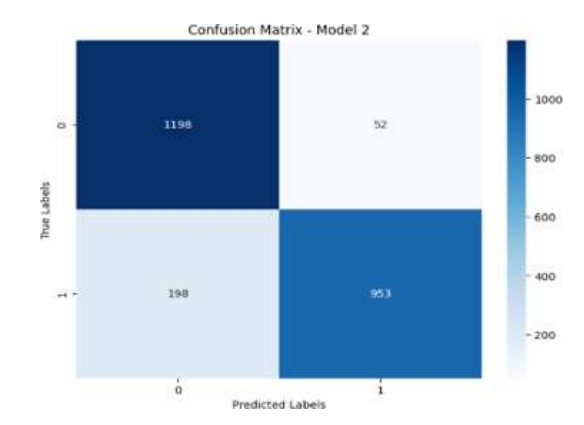


Figure 22. Confusion matrix of the second model

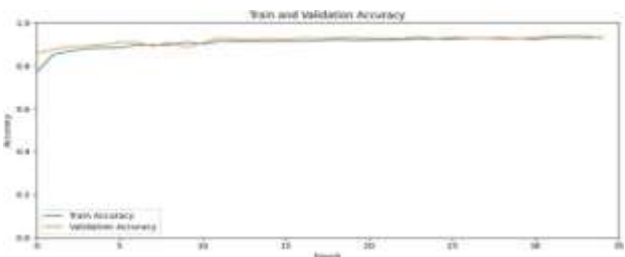


Figure. 23. Accuracy curves as a function of training epochs for the third model

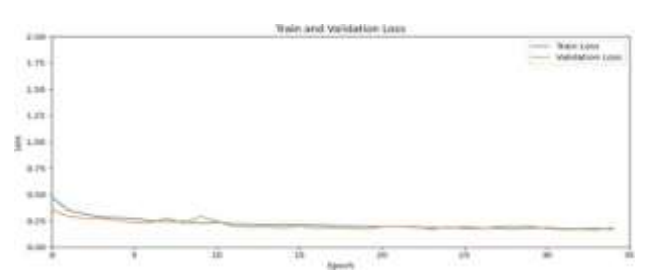


Figure. 24. Loss curves as a function of training epochs for the third model

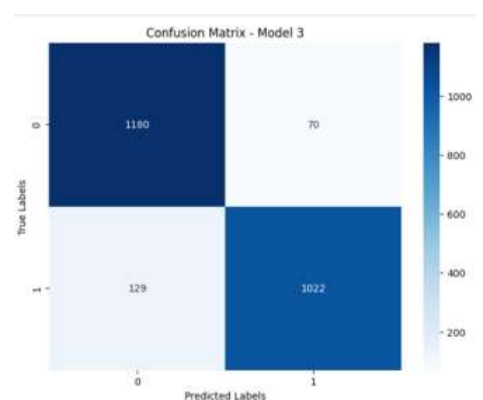


Figure. 25. Confusion matrix of the third model

#### B. Comparison between all models

After training all models for 35 epochs and saving all models. Table 6 shows an overall comparison between the models in terms of accuracy, precision, recall and f1 score.

TABLE VI. OVERALL COMPARISON BETWEEN ALL MODELS

| Metric      | Class     | First model | Second<br>model | Third<br>model |
|-------------|-----------|-------------|-----------------|----------------|
| Accurac     | Benign    | 92%         | 89%             | 95%            |
| y           | Malignant | 91%         | 88%             | 94%            |
| Precision - | Benign    | 89%         | 83%             | 93%            |
|             | Malignant | 93%         | 97%             | 92%            |
| Recall      | Benign    | 94%         | 93%             | 95%            |
|             | Malignant | 87%         | 78%             | 94%            |
| F1-score    | Benign    | 91.43%      | 87.71%          | 93.8%          |
|             | Malignant | 89.9%       | 86.47%          | 93.01%         |

Overall, the first model has a better balance between TPs and TNs indicating a more balanced performance. The second model shows improvement in identifying Malignant cases but has a higher rate of FNs. The third model has the highest TPs but also exhibits a higher rate of FNs and misclassifying Benign cases. All three models show relatively high performance for all metrics. for accuracy metric, the third model performs the best, followed by the first model, and then the second model. In the Benign class, the third model attains the highest precision indicating its effectiveness in precisely determining Benign instances. On the other hand, the second model exhibits a higher precision for the Malignant class reflecting its higher effectiveness in identifying Malignant cases. In the Benign class, the second model attains the highest recall, with equality in the recall performance of the first and third models. Nevertheless, in the Malignant class, the third model has the highest recall, and the second model obtains the lowest performance. For both classes, the third model obtains the highest F1-score, revealing a strong balance between recall and precision. Additionally, by taking the average results of both classes, the third model achieves the highest results for all metrics making the third model is the superior model in this paper.

Table 7 highlights key differences between our CNN model's performance and prior studies in skin lesion classification.

The paper demonstrates strong performance (94-95% accuracy) in line with contemporary CNN-based approaches, though it does not surpass hybrid or pretrained models like ResNet50+SVM. Future work could:

- Incorporate pretrained models (e.g., EfficientNet [29]) or ensemble methods (CNN+SVM [10]).
- Expand dataset diversity to address biases noted in [18].

TABLE VII. COMPARISON WITH OTHER STUDIES

|                                 |            |             |          |           | 1                           |   |
|---------------------------------|------------|-------------|----------|-----------|-----------------------------|---|
| Model                           | Accuracy % | Precision % | Recall % | F1-score% | Dataset                     | Notes   |
| My Study (Three<br>Models)      | % 56-76    | % £6-76     | 56-76    | % 8°86-86 | 10,602 images<br>(Kaggle)   | Custom CNN, 35<br>epochs, data<br>augmentation. |
| Sequential<br>CNN [9]           | % \$2.96   | -           | -        | -         | HAM 10,000                  | Outperformed<br>VGG19/ResNet<br>-50.            |
| SkinNet2<br>(CNN+SVM<br>) [10]  | 92 %       | ı           | ı        | ı         | Dermoscopy<br>images        | Hybrid<br>approach.                             |
| Modified<br>DenseNet201<br>[11] | % 5.56     | -           | % 96.£6  | -         | Skin lesion<br>images       | High sensitivity (97.03%).                      |
| ResNet50+SV<br>M [12]           | % 8.66     | 1           | 1        | 1         | Melanoma/beni<br>gn lesions | Best accuracy in literature.                    |
| VGG16<br>[15]                   | %          |             |          |           | Skin<br>lesions             | Transfer<br>learning.                           |
| MobileN<br>etV2 [17]            | 92.9 %     | 94.7 %      | 92.7 %   | 93.4 %    | Skin<br>lesions             | Lightweight<br>architecture.                    |

For clinical applications, the model's balanced precision/recall makes it a viable tool for early melanoma detection, complementing (but not replacing) Direct comparison is dermatologist assessments. challenging due to varying datasets/evaluation metrics, but the study's methodology and results hold significant value in the AI dermatology landscape.

Table 8 display the comparison of structure of three models to underscores the importance of architectural choices in medical image analysis, where model interpretability and reliability are as crucial as raw accuracy.

VIII. OVERALL COMPARISON BETWEEN ALL MODELS

| Feature          | Model 1                               | Model 2                               | Model 3                               |
|------------------|---------------------------------------|---------------------------------------|---------------------------------------|
| Architectur<br>e | 2 Conv<br>blocks                      | 4 Conv blocks                         | 4 Conv blocks (paired layers)         |
| Conv<br>Layers   | 2<br>(64, 128 filters)                | 4 (64, 128,<br>256, 512<br>filters)   | 4 (64→128 filters, paired)            |
| Dropout<br>Rates | 10% (1st layer),<br>15% (2nd)         | 10%, 15%,<br>20%, 30%<br>(per block)  | 50% (final FC layer)                  |
| Pooling          | MaxPool after<br>each conv            | MaxPool after<br>each conv            | MaxPool after<br>paired conv          |
| FC Layers        | $256 \rightarrow 2$ neurons           | $1024 \rightarrow 2$<br>neurons       | $256 \rightarrow 2$ neurons           |
| Activation       | Leaky ReLU<br>(Conv), Sigmoid<br>(FC) | Leaky ReLU<br>(Conv),<br>Sigmoid (FC) | Leaky ReLU<br>(Conv),<br>Sigmoid (FC) |
| Best<br>Accuracy | 91%<br>(Malignant),<br>92% (Benign)   | 88%<br>(Malignant),<br>89% (Benign)   | 94%<br>(Malignant),<br>95% (Benign)   |
| Key<br>Strength  | Balanced precision/recall             | High precision for malignant          | Best overall performance              |
| Limitation       | High benign<br>misclassification<br>s | Lower recall for malignant            | Slowest convergence                   |

The third model's architectural innovations—paired convolutions, strategic dropout, and balanced depth—demonstrate that thoughtful design choices can outperform deeper or more complex networks. These insights pave the way for more efficient, reliable, and deployable CNN models in dermatology and other medical imaging applications, ultimately bridging the gap between AI research and clinical utility.

#### 1. Layer Configuration and Depth

- The third model uses four convolutional layers arranged in two sequential convolution blocks, where each block has two conv layers followed by a pooling layer.
- This structure enables better hierarchical feature extraction:
  - The first conv layer captures basic features like edges or textures.
  - The second refines or combines them into more abstract patterns relevant to melanoma (e.g., irregular borders, pigmentation).
- Compared to the first model's shallow twolayer structure and second model's single-

layer-per-block design, this deeper and denser setup in the third model helps it learn more complex and high-level features.

#### 2. Use of Leaky RELU

- All models use Leaky ReLU, but the third model benefits more because it:
  - Prevents neuron deactivation (dying ReLU problem).
  - Enhances gradient flow, especially in deeper networks.

#### 3. High Dropout Rate in FC Layer (50%)

- The third model includes a 50% dropout layer before the final dense layer.
  - This is much higher than the 10–30% used in the other models.
  - It strongly regularizes the model, reducing overfitting and improving generalization.
- Dropout at this stage helps the network avoid reliance on a specific subset of features, which is important in noisy and diverse medical image data.

#### 4. Spatial Preservation via 'Same' Padding

- The model uses 'same' padding in the initial convolutional layers, which maintains spatial resolution.
  - This ensures more granular feature maps early in the network—important for recognizing small, detailed lesion features like jagged edges or uneven textures.

#### 5. Stable Learning Behavior

- As noted in the paper, the third model showed slow but steady learning curves and minimal overfitting between train and validation sets.
  - This indicates a well-balanced bias-variance tradeoff, essential for high test-time accuracy.

#### V. CONCLUSION

Among all cancers, melanoma skin cancer is one of the most dangerous that has caused the largest number of deaths. However, skin cancer is more treatable in the early stages because it spreads gradually. Diagnosis of skin cancer is a very challenging and costly process, which gives extra importance to the development of an alternative method for early diagnosis. The goal of this paper is to develop an effective DL model for early diagnosis of Melanoma skin cancer using CNN models through Keras Sequential API. Three different CNN models were developed for classifying Benign and Malignant skin cancer. A total of 10602 dermatoscopic images were used in this study, and the dataset has been split into 90-10 for train and test. Further division of the train set into 25% validation was made. Several data augmentations were created. By training the models on the Melanoma skin cancer dataset for 35 epochs, the models provided relatively high accuracies on the validations: 91%, 88%, and 94% for the first, second, and third model, respectively. This is inclusive of the graph on loss and accuracy, confusion matrix, and wrong predictions. Besides that, precision, recall, and F1 score metrics were computed. Overall, the third model was the best of all models used. While the 35-epoch limit provided a standardized comparison, adopting early stopping could enhance efficiency and generalization. Future iterations of this work should integrate adaptive training protocols to optimize performance without arbitrary epoch constraints.

#### VI. FUTURE WORK

- Further investigations are required to evaluate this
  work in classifying skin cancer. Additionally,
  acquiring a larger, more diverse collection of highresolution dermatoscopic images of skin lesions can
  enhance the system's ability to generalize and
  remain robust.
- For future improvements other pretrained models can be used to enhance the accuracy of the systems.

#### REFERENCES

- [1] Y. Alsahafi, M. Kassem, and K. Hosny, "Skin-Net: a novel deep residual network for skin lesions classification using multilevel feature extraction and cross-channel correlation with detection of outlier," *Journal of Big Data*, vol. 10, no. 1, 2023. doi.org/10.1186/s40537-023-00769-6.
- [2] M. Dildar, et al., "Skin Cancer Detection: A Review Using Deep Learning Techniques," *Int. J. Environ. Res. Public Health*, vol. 18, no. 10, 2021.doi.org/10.3390/ijerph18105479.
- [3] M. Hossin, et al., "Melanoma skin cancer detection using deep learning and advanced regularizer," 2020 International Conference on Advanced Computer Science and Information Systems, ICACSIS 2020. doi.org/10.1109/ICACSIS51025.2020.9263118.
- [4] R. Ashraf, et al., "an efficient technique for skin cancer classification using deep learning," Proceedings - 23rd IEEE International Multi-Topic Conference, INMIC 2020, 2020. doi.org/10.1109/INMIC50486.2020.9318164.
- [5] M. Javaid, et al., "Significance of machine learning in healthcare: Features, pillars and applications," international journal of intelligent networks, 2022. doi.org/10.1016/j.ijin.2022.05.002.
- [6] R. Gangurde, et al., "Developing an Efficient Cancer Detection and Prediction Tool Using Convolution Neural Network Integrated with Neural Pattern Recognition," BioMed Research International, 2023. https://doi.org/10.1155/2023/6970256.
- [7] A. Abougarair, et al., "Breast Cancer Histopathology Images Detection," International Conference on Artificial Intelligence and its Applications in the Age of Digital Transformation, Springer conference, Nouakchott, Mauritania, 23-25April, 2024.
- [8] A. Oun, et al., "Deep Learning-Based Automated Approach for Classifying Bacterial Images," *International Journal of Robotics* and Control Systems, vol.4, no. 2, 2024. doi: 10.31763/ijrcs. v4i2.1423
- [9] A. Abdullah, K. Siddique, and T. Shaukat, "An intelligent mechanism to detect multi-factor skin cancer," Diagnostics, vol. 14, no. 13, p. 1359, 2024. doi: 10.3390/diagnostics14131359.
- [10] R. Islam, et al., "SkinNet: A CNN model for improved benign and malignant skin lesion detection," *Proc. IEEE Conf.*, 2024, pp. 231–236. doi: 10.1109/peeiacon63629.2024.10800037.
- [11] S. Isuhibany, et al., "Classification of skin cancer lesions using explainable deep learning," *Sensors*, vol. 22, no. 18, p. 6915, 2022. doi: 10.3390/s22186915.

- [12] W. Salma and A. Eltrass, "Automated deep learning approach for classification of malignant melanoma and benign skin lesions," *Multimedia Tools Appl.*, vol. 81, no. 22, pp. 32643–32660, 2022. doi: 10.1007/s11042-022-13081-x.
- [13] N. Lankadasu, D. Pesarlanka, A. Sharma, S. Sharma, and S. Gochhait, "Skin cancer classification using a convolutional neural network: An exploration into deep learning," Proc. IEEE Conf., 2024, pp. 1047–1052. doi: 0.1109/icetsis61505.2024.10459368.
- [14] M. Oumoulylte, A. Alaoui, Y. Farhaoui, A. El Allaoui, and A. Bahri, "Convolutional neural network-based approach for skin lesion classification," *Diagnostics*, 2023. doi: 10.56294/dm2023171.
- [15] M. Oumoulylte, A. O. Alaoui, Y. Farhaoui, A. El Allaoui, and A. Bahri, "Convolutional neural network-based skin cancer classification with transfer learning models," *Radioelektronnì i Komp'ûternì Sistemi*, 2023. doi: 10.32620/reks.2023.4.07.
- [16] S. Patil and H. Patil, "Modified CNNs for automated binary classification of skin lesions: Benign vs. malignant," *Proc. IEEE Conf.*, 2023, pp. 958–964. doi: 10.1109/aece59614.2023.10428444.
- [17] E. Aslan and Y. Özüpak, "Advanced skin cancer detection using convolutional neural networks and transfer learning," *Middle East J. Sci.*, 2024. doi: 10.51477/mejs.1592302.
- [18] A. John-Otumu, R. Ekemonye, T. Ewunonu, V. O. Aniugo, and O. Okonkwo, "Optimizing CNN kernel sizes for enhanced melanoma lesion classification in dermoscopy images," *Mach. Learn. Res.*, vol. 9, no. 2, pp. 26–38, 2024. doi: 10.11648/j.mlr.20240902.11.
- [19] N. Lankadasu, D. Pesarlanka, "A. Sharma, S. Sharma, and S. Gochhait, "Skin cancer classification using a convolutional neural network: An exploration into deep learning," *Proc. IEEE Conf.*, 2024, pp. 1047–1052. doi: 10.1109/icetsis61505.2024.10459368.
- [20] J. Seetha, et al., "Computer-aided detection of skin cancer detection from lesion images via deep-learning techniques," *Int. J. Recent Innov. Trends Comput. Commun.*, vol. 11, no. 2s, pp. 293–302, 2023. doi: 10.17762/ijritcc.v11i2s.6158.
- [21] S. Al-Sultan, "Deep learning-based automated diagnosis of skin cancer from thermoscopic images," *J. Univ. Babylon*, vol. 32, no. 4, pp. 199–212, 2024. doi: 10.29196/jubpas. v32i4.5533.
- [22] M. Singla, K. Gill, M. Kumar, and R. Rawat, "Cutting-edge dermatological advances using deep learning for precise skin cancer classification," *Proc. IEEE Conf.*, 2024. doi: 10.1109/icsses62373.2024.10561393.
- [23] E. Hamed, M. Salem, N. Badr, and M. Tolba, "A deep learning-based classification framework for annotated histopathology lung cancer images," *Proc. Int. Conf.*, 2023, pp. 86–94. doi: 10.1007/978-3-031-43247-7 8.
- [24] H. Nair, et al., "Melanoma skin cancer prediction using machine learning algorithm," *Deleted J.*, vol. 2, no. 12, pp. 3703–3709, 2024. doi: 10.47392/irjaem.2024.0550.
- [25] T. Mahmood, J. Li, Y. Pei, F. Akhtar, M. Rehman, and S. Wasti, "Breast lesions classifications of mammographic images using a deep convolutional neural network-based approach," *PLOS ONE*, vol. 17, no. 1, p. e0263126, 2022. doi: 10.1371/journal.pone.0263126.
- [26] A. Ajel, A. Al-Dujaili, Z. G. Hadi, and A. J. Humaidi, "Skin cancer classifier based on convolution residual neural network," Int. J. Electr. Comput. Eng., vol. 13, no. 6, pp. 6240–6248, 2023. doi: 10.11591/ijece. v13i6.pp6240-6248.
- [27] T. Nivyashree and P. V. Pramila, "Detection of malignant and benign skin lesions using the influence of activation function and accuracy analysis in densely connected convolutional network compared over convolutional neural network," *Proc. IEEE Conf.*, 2023, pp. 1–6. doi: 10.1109/iccebs58601.2023.10448550.
- [28] R. Sahu and A. Dash, "Identification of malignant cells using convolutional neural network," in *Proc. IEEE Conf.*, 2023, pp. 01– 06. doi: 10.1109/ccpis59145.2023.10291907.
- [29] R. Mhedbi, H. Chan, P. Credico, R. Joshi, J. Wong, and C. Hong, "A convolutional neural network-based system for classifying malignant and benign skin lesions using mobile-device images," medRxiv, 2023. doi: 10.1101/2023.12.06.23299413.
- [30] M. Abugarir, et al., CNNs for Automatic Skin Cancer Classification," Journal of Advances in Artificial Intelligence, Vol. 2, Num. 2, 2024.doi: 10.18178/JAAI.2024.2.2.218-234
- [31] F. Thabit, et al., "Blood Cells Cancer Detection Based on Deep Learning," *Journal of Advances in Artificial Intelligence*, Volume 2, Number 1, 2024. DOI: 10.18178/JAAI.2024.2.1.108-121.

- [32] C. Fanconi, Skin cancer: malignant vs. Benign, processed skin cancer pictures of the ISIC archive Kaggle dataset, https://www.kaggle.com/fanconic/skin-cancer-malignant-vs benign.
- [33] M. Dildar, S. Akram, M. Irfan et al., "Skin cancer detection: a review using deep learning techniques," *International Journal of Environmental Research and Public Health*, vol. 18, no. 10, pp. 1–22, 2021.
- [34] M. Hasan, et al., "Skin cancer detection using convolutional neural network," Proceedings of the 2019 5th International Conference on Computing and Artificial Intelligence-ICCAI 19, pp. 254–258, Association for Computing Machinery, New York, NY, USA, 2019.
- [35] T. Yue, et al., "An experimental study on breast lesion detection and classification from ultrasound images using deep learning architectures," BMC Medical Imaging, vol. 19, no. 1, 2019.
- [36] O. Salih, et al., "FFT-Assisted U-Net Architecture for Improved Skin Lesion Segmentation," *IEEE 3rd International Maghreb Meeting of the Conference on Sciences and Techniques of Automatic Control and Computer Engineering (MI-STA2023)*, 21-23 May,2023, Benghazi, Libya.
- [37] O. Salih, et al., "An Overview of Skin Lesion Segmentation Methods: Techniques, Challenges, and Future Directions," *IEEE 3rd International Maghreb Meeting of the Conference on Sciences and Techniques of Automatic Control and Computer Engineering (MI-STA2023)*, 21-23 May,2023, Benghazi, Libya.
- [38] S. Elghany, et al., "Diagnosis of various skin cancer lesions based on fine-tuned Resnet50 deep network, Computers," *Materials & Continua*, vol. 68, no. 1, pp. 117–135, 2021.
- [39] D. Renza, et al., "Fake banknote recognition using deep learning," Applied Sciences, vol. 11, no. 3, p. 1281, 2021.
- [40] A. Abougarair, "Optimal Control Synthesis of Epidemic Model," IJEIT International Journal on Engineering and Information Technology, vol.8, no. 2, Misrata, June 2022, Special Issue for the International Engineering Conference IEC2022 MU.
- [41] W. Elside, "Traffic Sign Recognition Using CNN," Journal of Advances in Artificial Intelligences, Vol.3, Number 1, 2025.
- [42] M. Bakouri, et al. "Optimizing cancer treatment using optimal control theory," AIMS Mathematics, 2024, Volume 9, Issue 11: 31740-31769. doi: 10.3934/math.20241526
- [43] S. Sawan, et al., "Cancer Treatment Precision Strategies Through Optimal Control Theory," *Journal of Robotics and Control (JRC)*, Vol. 5, Issue 5, pp. 1261-1290, 2024.
- [44] I. Alkaber, et al., "Comparative Evaluation of PID Controller Tuning through Conventional and Genetic Algorithm," IEEE 4th International Maghreb Meeting of the Conference on Sciences and Techniques of Automatic Control and Computer Engineering (MI-STA), Tripoli, Libya, 19-21 May 2024.
- [45] S. Elwefati, et al., "Identification and Control of Epidemic Disease Based Neural Networks and Optimization Technique," International Journal of Robotics and Control Systems, 3(4),780-803, 2023.
- [46] A. Ma'arif, et al., "Model Predictive Control for Optimizes Battery Charging Process," IEEE 4th International Maghreb Meeting of the Conference on Sciences and Techniques of Automatic Control and Computer Engineering (MI-STA), Tripoli, Libya, 19-21 May 2024.
- [47] A. Abougarair, "Adaptive Neural Networks Based Optimal Control for Stabilizing Nonlinear System," *IEEE 3rd International Maghreb Meeting of the Conference on Sciences and Techniques of Automatic Control and Computer Engineering (MI-STA2023)*, 21-23 May,2023, Benghazi, Libya.
- [48] I. Buzkhar, "Modeling and Control of a Two-Wheeled Robot Machine with a Handling Mechanism," *IEEE 3rd International Maghreb Meeting of the Conference on Sciences and Techniques of Automatic Control and Computer Engineering (MI-STA2023)*, 21-23 May,2023, Benghazi, Libya.
- [49] A. Abougarair, "Real Time Classification for Robotic Arm Control Based Electromyographic Signal, 2022 IEEE 2st International Maghreb Meeting of the Conference on Sciences and Techniques of Automatic Control and Computer Engineering (MI-STA2022), 23-25 may,2022, Sabrata, Libya.

- [50] M. Aburakhis, et al., "Adaptive Neural Networks Based Robust Output Feedback Controllers for Nonlinear Systems," International Journal of Robotics and Control Systems, Vol. 2, No.1, 2022, pp. 37-56, ISSN: 2775-2658, http://pubs2.ascee.org/index.php/ijrcs
- [51] M. Bakush, et al., "Control of Epidemic Disease Based Optimization Technique," IEEE 1st International Maghreb Meeting of the Conference on Sciences and Techniques of Automatic Control and Computer Engineering (MI-STA2021),25-27 may,2021, Tripoli, Libya.
- [52] H. Gnan, et al., "Implementation of a Brain-Computer Interface for Robotic Arm Control," IEEE 1st International Maghreb Meeting of the Conference on Sciences and Techniques of Automatic Control and Computer Engineering (MI-STA2021),25-27 may,2021, Tripoli, Libya.
- [53] A. Abougarair, "Position and Orientation Control of a Mobile Robot Using Intelligent Algorithms Based Hybrid Control Strategies," *Journal of Engineering Research*, Issue (34), pp 67-86, September 2022.
- [54] A. Abougarair, "Model Reference Adaptive Control And Fuzzy Optimal Controller For Mobile Robot," *Journal of Multidisciplinary Engineering Science and Technology*, pp 9722-9728, Vol. 6, Issue 3, 2019, Germany.
- [55] M. Edardar et al., "Tracking control with hysteresis compensation using neural networks," 2021 IEEE 1st International Maghreb Meeting of the Conference on Sciences and Techniques of Automatic Control and Computer Engineering MI-STA, pp. 36-40, 25-27 May 2021.
- [56] M. Edardar et al., "Lyapunov Redesign of Piezo-Actuator for Positioning Control," 9th International Conference on Systems and Control (ICSC), Caen, France, pp. 499-503, 2021.
  [57] W. Arebi et. al., "Smart glove for sign language translation,"
- [57] W. Arebi et. al., "Smart glove for sign language translation," International Robotics & Automation Journal, vol. 8, issue 3, pp. 109-117, 2022.